Search for $D^0 - \bar{D}^0$ mixing using doubly flavor tagged semileptonic decay modes

B. Aubert,[1] M. Bona,[1] D. Boutigny,[1] Y. Karyotakis,[1] J. P. Lees,[1] V. Poireau,[1] X. Prudent,[1] V. Tisserand,[1] A. Zghiche,[1]
J. Garra Tico,[2] E. Grauges,[2] L. Lopez,[3] A. Palano,[3] G. Eigen,[4] B. Stugu,[4] L. Sun,[4] G. S. Abrams,[5] M. Battaglia,[5]
D. N. Brown,[5] J. Button-Shafer,[5] R. N. Cahn,[5] Y. Groysman,[5] R. G. Jacobsen,[5] J. A. Kadyk,[5] L. T. Kerth,[5]
Yu. G. Kolomensky,[5] G. Kukartsev,[5] D. Lopes Pegna,[5] G. Lynch,[5] L. M. Mir,[5] T. J. Orimoto,[5] M. T. Ronan,[5,*]
K. Tackmann,[5] W. A. Wenzel,[5] P. del Amo Sanchez,[6] C. M. Hawkes,[6] A. T. Watson,[6] T. Held,[7] H. Koch,[7]
B. Lewandowski,[7] M. Pelizaeus,[7] T. Schroeder,[7] M. Steinke,[7] D. Walker,[8] D. J. Asgeirsson,[9] T. Cuhadar-Donszelmann,[9]
B. G. Fulsom,[9] C. Hearty,[9] N. S. Knecht,[9] T. S. Mattison,[9] J. A. McKenna,[9] A. Khan,[10] M. Saleem,[10] L. Teodorescu,[10]
V. E. Blinov,[11] A. D. Bukin,[11] V. P. Druzhinin,[11] V. B. Golubev,[11] A. P. Onuchin,[11] S. I. Serednyakov,[11] Yu. I. Skovpen,[11]
E. P. Solodov,[11] K. Yu Todyshev,[11] M. Bondioli,[12] S. Curry,[12] I. Eschrich,[12] D. Kirkby,[12] A. J. Lankford,[12] P. Lund,[12]
M. Mandelkern,[12] E. C. Martin,[12] D. P. Stoker,[12] S. Abachi,[13] C. Buchanan,[13] S. D. Foulkes,[14] J. W. Gary,[14] F. Liu,[14]
O. Long,[14] B. C. Shen,[14] L. Zhang,[14] H. P. Paar,[15] S. Rahatlou,[15] V. Sharma,[15] J. W. Berryhill,[16] C. Campagnari,[16]
A. Cunha,[16] B. Dahmes,[16] T. M. Hong,[16] D. Kovalskyi,[16] J. D. Richman,[16] T. W. Beck,[17] A. M. Eisner,[17] C. J. Flacco,[17]
C. A. Heusch,[17] J. Kroseberg,[17] W. S. Lockman,[17] T. Schalk,[17] B. A. Schumm,[17] A. Seiden,[17] D. C. Williams,[17]
M. G. Wilson,[17] L. O. Winstrom,[17] E. Chen,[18] C. H. Cheng,[18] F. Fang,[18] D. G. Hitlin,[18] I. Narsky,[18] T. Piatenko,[18]
F. C. Porter,[18] G. Mancinelli,[19] B. T. Meadows,[19] K. Mishra,[19] M. D. Sokoloff,[19] F. Blanc,[20] P. C. Bloom,[20] S. Chen,[20]
W. T. Ford,[20] J. F. Hirschauer,[20] A. Kreisel,[20] M. Nagel,[20] U. Nauenberg,[20] A. Olivas,[20] J. G. Smith,[20] K. A. Ulmer,[20]
S. R. Wagner,[20] J. Zhang,[20] A. M. Gabareen,[21] A. Soffer,[21] W. H. Toki,[21] R. J. Wilson,[21] F. Winklmeier,[21] Q. Zeng,[21]
D. D. Altenburg,[22] E. Feltresi,[22] A. Hauke,[22] H. Jasper,[22] J. Merkel,[22] A. Petzold,[22] B. Spaan,[22] K. Wacker,[22] T. Brandt,[23]
V. Klose,[23] M. J. Kobel,[23] H. M. Lacker,[23] W. F. Mader,[23] R. Nogowski,[23] J. Schubert,[23] K. R. Schubert,[23] R. Schwierz,[23]
J. E. Sundermann,[23] A. Volk,[23] D. Bernard,[24] G. R. Bonneaud,[24] E. Latour,[24] V. Lombardo,[24] Ch. Thiebaux,[24]
M. Verderi,[24] P. J. Clark,[25] W. Gradl,[25] F. Muheim,[25] S. Playfer,[25] A. I. Robertson,[25] Y. Xie,[25] M. Andreotti,[26] D. Bettoni,[26]
C. Bozzi,[26] R. Calabrese,[26] A. Cecchi,[26] G. Cibinetto,[26] P. Franchini,[26] E. Luppi,[26] M. Negrini,[26] A. Petrella,[26]
L. Piemontese,[26] E. Prencipe,[26] V. Santoro,[26] F. Anulli,[27] R. Baldini-Ferroli,[27] A. Calcaterra,[27] R. de Sangro,[27]
G. Finocchiaro,[27] S. Pacetti,[27] P. Patteri,[27] I. M. Peruzzi,[27,†] M. Piccolo,[27] M. Rama,[27] A. Zallo,[27] A. Buzzo,[28] R. Contri,[28]
M. Lo Vetere,[28] M. M. Macri,[28] M. R. Monge,[28] S. Passaggio,[28] C. Patrignani,[28] E. Robutti,[28] A. Santroni,[28] S. Tosi,[28]
K. S. Chaisanguanthum,[29] M. Morii,[29] J. Wu,[29] R. S. Dubitzky,[30] J. Marks,[30] S. Schenk,[30] U. Uwer,[30] D. J. Bard,[31]
P. D. Dauncey,[31] R. L. Flack,[31] J. A. Nash,[31] M. B. Nikolich,[31] W. Panduro Vazquez,[31] P. K. Behera,[32] X. Chai,[32]
M. J. Charles,[32] U. Mallik,[32] N. T. Meyer,[32] V. Ziegler,[32] J. Cochran,[33] H. B. Crawley,[33] L. Dong,[33] V. Eyges,[33]
W. T. Meyer,[33] S. Prell,[33] E. I. Rosenberg,[33] A. E. Rubin,[33] A. V. Gritsan,[34] Z. J. Guo,[34] C. K. Lae,[34] A. G. Denig,[35]
M. Fritsch,[35] G. Schott,[35] N. Arnaud,[36] J. Béquilleux,[36] M. Davier,[36] G. Grosdidier,[36] A. Höcker,[36] V. Lepeltier,[36]
F. Le Diberder,[36] A. M. Lutz,[36] S. Pruvot,[36] S. Rodier,[36] P. Roudeau,[36] M. H. Schune,[36] J. Serrano,[36] V. Sordini,[36]
A. Stocchi,[36] W. F. Wang,[36] G. Wormser,[36] D. J. Lange,[37] D. M. Wright,[37] C. A. Chavez,[38] I. J. Forster,[38] J. R. Fry,[38]
E. Gabathuler,[38] R. Gamet,[38] D. E. Hutchcroft,[38] D. J. Payne,[38] K. C. Schofield,[38] C. Touramanis,[38] A. J. Bevan,[39]
K. A. George,[39] F. Di Lodovico,[39] W. Menges,[39] R. Sacco,[39] G. Cowan,[40] H. U. Flaecher,[40] D. A. Hopkins,[40]
P. S. Jackson,[40] T. R. McMahon,[40] F. Salvatore,[40] A. C. Wren,[40] D. N. Brown,[41] C. L. Davis,[41] J. Allison,[42] N. R. Barlow,[42]
R. J. Barlow,[42] Y. M. Chia,[42] C. L. Edgar,[42] G. D. Lafferty,[42] T. J. West,[42] J. I. Yi,[42] J. Anderson,[43] C. Chen,[43]
A. Jawahery,[43] D. A. Roberts,[43] G. Simi,[43] J. M. Tuggle,[43] G. Blaylock,[44] C. Dallapiccola,[44] S. S. Hertzbach,[44] X. Li,[44]
T. B. Moore,[44] E. Salvati,[44] S. Saremi,[44] R. Cowan,[45] P. H. Fisher,[45] G. Sciolla,[45] S. J. Sekula,[45] M. Spitznagel,[45]
F. Taylor,[45] R. K. Yamamoto,[45] S. E. Mclachlin,[46] P. M. Patel,[46] S. H. Robertson,[46] A. Lazzaro,[47] F. Palombo,[47]
J. M. Bauer,[48] L. Cremaldi,[48] V. Eschenburg,[48] R. Godang,[48] R. Kroeger,[48] D. A. Sanders,[48] D. J. Summers,[48]
H. W. Zhao,[48] S. Brunet,[49] D. Côté,[49] M. Simard,[49] P. Taras,[49] F. B. Viaud,[49] H. Nicholson,[50] G. De Nardo,[51] F. Fabozzi,[51,‡]
L. Lista,[51] D. Monorchio,[51] C. Sciacca,[51] M. A. Baak,[52] G. Raven,[52] H. L. Snoek,[52] C. P. Jessop,[53] J. M. LoSecco,[53]
G. Benelli,[54] L. A. Corwin,[54] K. K. Gan,[54] K. Honscheid,[54] D. Hufnagel,[54] H. Kagan,[54] R. Kass,[54] J. P. Morris,[54]
A. M. Rahimi,[54] J. J. Regensburger,[54] R. Ter-Antonyan,[54] Q. K. Wong,[54] N. L. Blount,[55] J. Brau,[55] R. Frey,[55] O. Igonkina,[55]
J. A. Kolb,[55] M. Lu,[55] R. Rahmat,[55] N. B. Sinev,[55] D. Strom,[55] J. Strube,[55] E. Torrence,[55] N. Gagliardi,[56] A. Gaz,[56]
M. Margoni,[56] M. Morandin,[56] A. Pompili,[56] M. Posocco,[56] M. Rotondo,[56] F. Simonetto,[56] R. Stroili,[56] C. Voci,[56]
E. Ben-Haim,[57] H. Briand,[57] G. Calderini,[57] J. Chauveau,[57] P. David,[57] L. Del Buono,[57] Ch. de la Vaissière,[57] O. Hamon,[57]
Ph. Leruste,[57] J. Malclès,[57] J. Ocariz,[57] A. Perez,[57] L. Gladney,[58] M. Biasini,[59] R. Covarelli,[59] E. Manoni,[59] C. Angelini,[60]
G. Batignani,[60] S. Bettarini,[60] M. Carpinelli,[60] R. Cenci,[60] A. Cervelli,[60] F. Forti,[60] M. A. Giorgi,[60] A. Lusiani,[60]

G. Marchiori,[60] M. A. Mazur,[60] M. Morganti,[60] N. Neri,[60] E. Paoloni,[60] G. Rizzo,[60] J. J. Walsh,[60] M. Haire,[61] J. Biesiada,[62] P. Elmer,[62] Y. P. Lau,[62] C. Lu,[62] J. Olsen,[62] A. J. S. Smith,[62] A. V. Telnov,[62] E. Baracchini,[63] F. Bellini,[63] G. Cavoto,[63] A. D'Orazio,[63] D. del Re,[63] E. Di Marco,[63] R. Faccini,[63] F. Ferrarotto,[63] F. Ferroni,[63] M. Gaspero,[63] P. D. Jackson,[63] L. Li Gioi,[63] M. A. Mazzoni,[63] S. Morganti,[63] G. Piredda,[63] F. Polci,[63] F. Renga,[63] C. Voena,[63] M. Ebert,[64] H. Schröder,[64] R. Waldi,[64] T. Adye,[65] G. Castelli,[65] B. Franek,[65] E. O. Olaiya,[65] S. Ricciardi,[65] W. Roethel,[65] F. F. Wilson,[65] R. Aleksan,[66] S. Emery,[66] M. Escalier,[66] A. Gaidot,[66] S. F. Ganzhur,[66] G. Hamel de Monchenault,[66] W. Kozanecki,[66] M. Legendre,[66] G. Vasseur,[66] Ch. Yèche,[66] M. Zito,[66] X. R. Chen,[67] H. Liu,[67] W. Park,[67] M. V. Purohit,[67] J. R. Wilson,[67] M. T. Allen,[68] D. Aston,[68] R. Bartoldus,[68] P. Bechtle,[68] N. Berger,[68] R. Claus,[68] J. P. Coleman,[68] M. R. Convery,[68] J. C. Dingfelder,[68] J. Dorfan,[68] G. P. Dubois-Felsmann,[68] D. Dujmic,[68] W. Dunwoodie,[68] R. C. Field,[68] T. Glanzman,[68] S. J. Gowdy,[68] M. T. Graham,[68] P. Grenier,[68] C. Hast,[68] T. Hryn'ova,[68] W. R. Innes,[68] J. Kaminski,[68] M. H. Kelsey,[68] H. Kim,[68] P. Kim,[68] M. L. Kocian,[68] D. W. G. S. Leith,[68] S. Li,[68] S. Luitz,[68] V. Luth,[68] H. L. Lynch,[68] D. B. MacFarlane,[68] H. Marsiske,[68] R. Messner,[68] D. R. Muller,[68] C. P. O'Grady,[68] I. Ofte,[68] A. Perazzo,[68] M. Perl,[68] T. Pulliam,[68] B. N. Ratcliff,[68] A. Roodman,[68] A. A. Salnikov,[68] R. H. Schindler,[68] J. Schwiening,[68] A. Snyder,[68] J. Stelzer,[68] D. Su,[68] M. K. Sullivan,[68] K. Suzuki,[68] S. K. Swain,[68] J. M. Thompson,[68] J. Va'vra,[68] N. van Bakel,[68] A. P. Wagner,[68] M. Weaver,[68] W. J. Wisniewski,[68] M. Wittgen,[68] D. H. Wright,[68] A. K. Yarritu,[68] K. Yi,[68] C. C. Young,[68] P. R. Burchat,[69] A. J. Edwards,[69] S. A. Majewski,[69] B. A. Petersen,[69] L. Wilden,[69] S. Ahmed,[70] M. S. Alam,[70] R. Bula,[70] J. A. Ernst,[70] V. Jain,[70] B. Pan,[70] M. A. Saeed,[70] F. R. Wappler,[70] S. B. Zain,[70] W. Bugg,[71] M. Krishnamurthy,[71] S. M. Spanier,[71] R. Eckmann,[72] J. L. Ritchie,[72] A. M. Ruland,[72] C. J. Schilling,[72] R. F. Schwitters,[72] J. M. Izen,[73] X. C. Lou,[73] S. Ye,[73] F. Bianchi,[74] F. Gallo,[74] D. Gamba,[74] M. Pelliccioni,[74] M. Bomben,[75] L. Bosisio,[75] C. Cartaro,[75] F. Cossutti,[75] G. Della Ricca,[75] L. Lanceri,[75] L. Vitale,[75] V. Azzolini,[76] N. Lopez-March,[76] F. Martinez-Vidal,[76] D. A. Milanes,[76] A. Oyanguren,[76] J. Albert,[77] Sw. Banerjee,[77] B. Bhuyan,[77] K. Hamano,[77] R. Kowalewski,[77] I. M. Nugent,[77] J. M. Roney,[77] R. J. Sobie,[77] J. J. Back,[78] P. F. Harrison,[78] T. E. Latham,[78] G. B. Mohanty,[78] M. Pappagallo,[78,§] H. R. Band,[79] X. Chen,[79] S. Dasu,[79] K. T. Flood,[79] J. J. Hollar,[79] P. E. Kutter,[79] Y. Pan,[79] M. Pierini,[79] R. Prepost,[79] S. L. Wu,[79] Z. Yu,[79] and H. Neal[80]

(*BABAR* Collaboration)

[1]*Laboratoire de Physique des Particules, IN2P3/CNRS et Université de Savoie, F-74941 Annecy-Le-Vieux, France*
[2]*Universitat de Barcelona, Facultat de Fisica, Departament ECM, E-08028 Barcelona, Spain*
[3]*Università di Bari, Dipartimento di Fisica and INFN, I-70126 Bari, Italy*
[4]*University of Bergen, Institute of Physics, N-5007 Bergen, Norway*
[5]*Lawrence Berkeley National Laboratory and University of California, Berkeley, California 94720, USA*
[6]*University of Birmingham, Birmingham, B15 2TT, United Kingdom*
[7]*Ruhr Universität Bochum, Institut für Experimentalphysik 1, D-44780 Bochum, Germany*
[8]*University of Bristol, Bristol BS8 1TL, United Kingdom*
[9]*University of British Columbia, Vancouver, British Columbia, Canada V6T 1Z1*
[10]*Brunel University, Uxbridge, Middlesex UB8 3PH, United Kingdom*
[11]*Budker Institute of Nuclear Physics, Novosibirsk 630090, Russia*
[12]*University of California at Irvine, Irvine, California 92697, USA*
[13]*University of California at Los Angeles, Los Angeles, California 90024, USA*
[14]*University of California at Riverside, Riverside, California 92521, USA*
[15]*University of California at San Diego, La Jolla, California 92093, USA*
[16]*University of California at Santa Barbara, Santa Barbara, California 93106, USA*
[17]*University of California at Santa Cruz, Institute for Particle Physics, Santa Cruz, California 95064, USA*
[18]*California Institute of Technology, Pasadena, California 91125, USA*
[19]*University of Cincinnati, Cincinnati, Ohio 45221, USA*
[20]*University of Colorado, Boulder, Colorado 80309, USA*
[21]*Colorado State University, Fort Collins, Colorado 80523, USA*
[22]*Universität Dortmund, Institut für Physik, D-44221 Dortmund, Germany*
[23]*Technische Universität Dresden, Institut für Kern-und Teilchenphysik, D-01062 Dresden, Germany*
[24]*Laboratoire Leprince-Ringuet, CNRS/IN2P3, Ecole Polytechnique, F-91128 Palaiseau, France*
[25]*University of Edinburgh, Edinburgh EH9 3JZ, United Kingdom*
[26]*Università di Ferrara, Dipartimento di Fisica and INFN, I-44100 Ferrara, Italy*
[27]*Laboratori Nazionali di Frascati dell'INFN, I-00044 Frascati, Italy*
[28]*Università di Genova, Dipartimento di Fisica and INFN, I-16146 Genova, Italy*
[29]*Harvard University, Cambridge, Massachusetts 02138, USA*
[30]*Universität Heidelberg, Physikalisches Institut, Philosophenweg 12, D-69120 Heidelberg, Germany*

[31]Imperial College London, London, SW7 2AZ, United Kingdom

[32]University of Iowa, Iowa City, Iowa 52242, USA

[33]Iowa State University, Ames, Iowa 50011-3160, USA

[34]Johns Hopkins University, Baltimore, Maryland 21218, USA

[35]Universität Karlsruhe, Institut für Experimentelle Kernphysik, D-76021 Karlsruhe, Germany

[36]Laboratoire de l'Accélérateur Linéaire, IN2P3/CNRS et Université Paris-Sud 11,
Centre Scientifique d'Orsay, B. P. 34, F-91898 ORSAY Cedex, France

[37]Lawrence Livermore National Laboratory, Livermore, California 94550, USA

[38]University of Liverpool, Liverpool L69 7ZE, United Kingdom

[39]Queen Mary, University of London, E1 4NS, United Kingdom

[40]University of London, Royal Holloway and Bedford New College, Egham, Surrey TW20 0EX, United Kingdom

[41]University of Louisville, Louisville, Kentucky 40292, USA

[42]University of Manchester, Manchester M13 9PL, United Kingdom

[43]University of Maryland, College Park, Maryland 20742, USA

[44]University of Massachusetts, Amherst, Massachusetts 01003, USA

[45]Massachusetts Institute of Technology, Laboratory for Nuclear Science, Cambridge, Massachusetts 02139, USA

[46]McGill University, Montréal, Québec, Canada H3A 2T8

[47]Università di Milano, Dipartimento di Fisica and INFN, I-20133 Milano, Italy

[48]University of Mississippi, University, Mississippi 38677, USA

[49]Université de Montréal, Physique des Particules, Montréal, Québec, Canada H3C 3J7

[50]Mount Holyoke College, South Hadley, Massachusetts 01075, USA

[51]Università di Napoli Federico II, Dipartimento di Scienze Fisiche and INFN, I-80126, Napoli, Italy

[52]NIKHEF, National Institute for Nuclear Physics and High Energy Physics, NL-1009 DB Amsterdam, The Netherlands

[53]University of Notre Dame, Notre Dame, Indiana 46556, USA

[54]Ohio State University, Columbus, Ohio 43210, USA

[55]University of Oregon, Eugene, Oregon 97403, USA

[56]Università di Padova, Dipartimento di Fisica and INFN, I-35131 Padova, Italy

[57]Laboratoire de Physique Nucléaire et de Hautes Energies, IN2P3/CNRS, Université Pierre et Marie Curie-Paris6,
Université Denis Diderot-Paris7, F-75252 Paris, France

[58]University of Pennsylvania, Philadelphia, Pennsylvania 19104, USA

[59]Università di Perugia, Dipartimento di Fisica and INFN, I-06100 Perugia, Italy

[60]Università di Pisa, Dipartimento di Fisica, Scuola Normale Superiore and INFN, I-56127 Pisa, Italy

[61]Prairie View A&M University, Prairie View, Texas 77446, USA

[62]Princeton University, Princeton, New Jersey 08544, USA

[63]Università di Roma La Sapienza, Dipartimento di Fisica and INFN, I-00185 Roma, Italy

[64]Universität Rostock, D-18051 Rostock, Germany

[65]Rutherford Appleton Laboratory, Chilton, Didcot, Oxon, OX11 0QX, United Kingdom

[66]DSM/Dapnia, CEA/Saclay, F-91191 Gif-sur-Yvette, France

[67]University of South Carolina, Columbia, South Carolina 29208, USA

[68]Stanford Linear Accelerator Center, Stanford, California 94309, USA

[69]Stanford University, Stanford, California 94305-4060, USA

[70]State University of New York, Albany, New York 12222, USA

[71]University of Tennessee, Knoxville, Tennessee 37996, USA

[72]University of Texas at Austin, Austin, Texas 78712, USA

[73]University of Texas at Dallas, Richardson, Texas 75083, USA

[74]Università di Torino, Dipartimento di Fisica Sperimentale and INFN, I-10125 Torino, Italy

[75]Università di Trieste, Dipartimento di Fisica and INFN, I-34127 Trieste, Italy

[76]IFIC, Universitat de Valencia-CSIC, E-46071 Valencia, Spain

[77]University of Victoria, Victoria, British Columbia, Canada V8W 3P6

[78]Department of Physics, University of Warwick, Coventry CV4 7AL, United Kingdom

[79]University of Wisconsin, Madison, Wisconsin 53706, USA

[80]Yale University, New Haven, Connecticut 06511, USA

We have searched for $D^0 - \bar{D}^0$ mixing in $D^{*+} \rightarrow \pi^+ D^0$ decays with $D^0 \rightarrow K^{(*)} e \nu$ in a sample of $e^+ e^- \rightarrow c \bar{c}$ events produced near 10.58 GeV. The charge of the slow pion from charged D^* decay tags the

———

[*]Deceased

[†]Also with Università di Perugia, Dipartimento di Fisica, Perugia, Italy

[‡]Also with Università della Basilicata, Potenza, Italy

[§]Also with IPPP, Physics Department, Durham University, Durham DH1 3LE, United Kingdom

charm flavor at production, and it is required to be consistent with the flavor of a fully reconstructed second charm decay in the same event. We observe 3 mixed candidates compared to 2.85 background events expected from simulation. We ascribe a 50% systematic uncertainty to this expected background rate. We find a central value for the mixing rate of 0.4×10^{-4}. Using a frequentist method, we set corresponding 68% and 90% confidence intervals at $(-5.6, 7.4) \times 10^{-4}$ and $(-13, 12) \times 10^{-4}$, respectively.

I. INTRODUCTION

The D^0 and $\bar{D}^0$ mesons are flavor eigenstates which are invariant in strong interactions but which are subject to electroweak interactions that allow an initially pure state to evolve into a time-dependent mixture of D^0 and $\bar{D}^0$. In the standard model (SM), such oscillations proceed through both short-distance and long-distance, nonperturbative amplitudes. The expected mixing rate mediated by down-type quark box diagrams [1] and di-penguin [2] diagrams is $\mathcal{O}(10^{-8}\text{–}10^{-10})$, well below the current experimental sensitivity of $\mathcal{O}(10^{-4}\text{–}10^{-3})$ [3]. The expected range for nonperturbative, long-distance contributions [3] is approximately bounded by the box diagram rate and the current experimental sensitivity. New physics predictions span the same large range [4]. While the presence of a mixing signal alone would not be a clear indication of new physics, the current experimental results already constrain many such models.

Because $D^0 - \bar{D}^0$ mixing has been considered a potential signature for new physics, and because CP violation in mixing would be indicative of new physics, there have been many mixing searches. Typically, these use samples of neutral D mesons which originate in charged D^* decays where the initial production flavor of the neutral D meson is tagged by the charge of the associated slow pion (π_s) D^{*+} daughter. In $D^0 \to K^{(*)} e\nu$ decays, the final flavor of the neutral D meson is uniquely identified by the charge of the lepton. The signs of the slow pion and lepton charges are the same for unmixed decays and they differ for mixed decays. Historically, these two classes of decays are denoted as *right sign* (RS) and *wrong sign* (WS), respectively.

Charm mixing is generally characterized by two dimensionless parameters, $x \equiv \Delta m / \Gamma$ and $y \equiv \Delta \Gamma / 2\Gamma$, where $\Delta m = m_2 - m_1$ ($\Delta \Gamma = \Gamma_2 - \Gamma_1$) is the mass (width) difference between the two neutral D mass eigenstates and Γ is the average width. If either x or y is nonzero, then $D^0 - \bar{D}^0$ mixing will occur. The decay time distribution of a neutral D meson which changes flavor and decays semileptonically (thus involving no interfering doubly Cabibbo-suppressed [DCS] amplitudes) is [5]:

$$R_{\text{mix}}(t) \cong R_{\text{unmix}}(t) \frac{x^2 + y^2}{4} \left(\frac{t}{\tau_{D^0}} \right)^2, \qquad (1)$$

where t is the proper time of the D^0 decay, τ_{D^0} is the characteristic D^0 lifetime ($= 1/\Gamma$), $R_{\text{unmix}}(t) \propto e^{-t/\tau_{D^0}}$, and the approximation is valid in the limit of small mixing rates. Sensitivity to x and y individually is lost with semileptonic final states. The time-integrated mixing rate r_{mix} relative to the unmixed rate is

$$r_{\text{mix}} = \frac{x^2 + y^2}{2}. \qquad (2)$$

The B-factory experiments have searched for $D^0 - \bar{D}^0$ mixing using semileptonic (SL) decays, where the initial flavor of the neutral D meson is tagged by the charge of the slow pion from a $D^{*\pm}$ decay. The limits on r_{mix} from these experiments [6,7] and CLEO [8] are listed in Table I, along with results from recently published searches for $D^0 - \bar{D}^0$ mixing using hadronic decay modes [9–13]. In the earlier

TABLE I. Mixing results from earlier measurements in e^+e^- experiments. The 384 fb^{-1} *BABAR* result assumes a zero strong phase between Cabbibo-favored and DCS WS $K\pi$ final states. The 540 fb^{-1} Belle result assumes CP conservation. Where errors are given, the first and second quoted errors are statistical and systematic, respectively.

Experiment	Decay mode	Integrated luminosity	Result
BABAR [6]	$D^0 \to K^{(*)-} e^+ \nu$	87 fb^{-1}	$r_{\text{mix}} < 42 \times 10^{-4}$ (90% CL)
Belle [7]	$D^0 \to K^{(*)-} e^+ \nu$	254 fb^{-1}	$r_{\text{mix}} < 10 \times 10^{-4}$ (90% CL)
CLEO [8]	$D^0 \to K^{(*)-} e^+ \nu$	9 fb^{-1}	$r_{\text{mix}} < 78 \times 10^{-4}$ (90% CL)
CLEO [9]	$D^0 \to K^0_S \pi^- \pi^+$	9 fb^{-1}	$r_{\text{mix}} < 63 \times 10^{-4}$ (95% CL)
Belle [10]	$D^0 \to K^+ \pi^-$	400 fb^{-1}	$r_{\text{mix}} < 4.0 \times 10^{-4}$ (95% CL)
BABAR [11]	$D^0 \to K^+ \pi^- \pi^0$	230 fb^{-1}	$r_{\text{mix}} < 5.4 \times 10^{-4}$ (95% CL)
BABAR [12]	$D^0 \to K^+ \pi^-$	384 fb^{-1}	$y = (9.7 \pm 4.4 \pm 3.1) \times 10^{-3}$
			$x^2 = (-0.22 \pm 0.30 \pm 0.21) \times 10^{-3}$
Belle [13]	$D^0 \to K^+ K^-, \pi^+ \pi^-$	540 fb^{-1}	$y = (13.1 \pm 3.2 \pm 2.5) \times 10^{-3}$

BABAR SL analysis [6], the dominant source of background in the WS signal channel originated from RS SL D^0 decays falsely associated with WS slow pion candidates. In this analysis we tag the initial flavor of the neutral D meson twice: once using the slow pion from the charged D^* decay from which the neutral D decays semileptonically, and once using the flavor of a high-momentum D fully reconstructed in the center-of-mass (CM) hemisphere opposite the semileptonic candidate. Tagging the flavor at production twice, rather than once, highly suppresses the background from false WS slow pions but also reduces the signal by more than an order of magnitude. The *BABAR* collaboration has previously used this tagging technique in a measurement of the pseudoscalar decay constant f_{Ds} [14]. We have implemented additional candidate selection criteria to minimize remaining sources of background, resulting in an estimated sensitivity for this double-tag analysis that is about the same as for a corresponding single-tag semileptonic analysis of the same data set.

II. THE *BABAR* DETECTOR AND DATA SET

The data used in this analysis were collected with the *BABAR* detector [15] at the PEP-II storage ring. The integrated luminosity used here is approximately 344 fb^{-1}, including running both at and just below the $Y(4S)$ resonance. Approximately 10% of the total data set was collected during off-resonance running. Charged-particle momenta are measured in a tracking system consisting of a five-layer double-sided silicon vertex tracker (SVT) and a 40-layer central drift chamber (DCH), both situated in a 1.5 T axial magnetic field. An internally reflecting ring-imaging Cherenkov detector (DIRC) with fused silica bar radiators provides charged-particle identification. A CsI(Tl) electromagnetic calorimeter (EMC) is used to detect and identify photons and electrons and measure their energies. Muons are identified in the instrumented flux return system.

Electron candidates are identified by the ratio of the energy deposited in the EMC to the measured track momentum, the shower shape, the specific ionization measured in the DCH, and the Cherenkov angle measured by the DIRC. Electron identification efficiency is greater than 90% at all momenta of interest here. Pion-as-electron misidentification rates increase from about 0.05% to 0.15% from 500 MeV/c to 3 GeV/c. Kaon-as-electron misidentification rates peak at about 2.5% near 500 MeV/c and decrease to 0.2% above 800 MeV/c.

Kaon candidates are selected using the specific ionization (dE/dx) measured in the DCH and SVT, and the Cherenkov angle measured in the DIRC. Kaon identification efficiency is a function of laboratory momentum; it is typically 80% or higher over the range 500 MeV/c to 3.5 GeV/c, with a maximum of about 90% at 2 GeV/c. The pion-as-kaon misidentification rate is typically 1% or

less for momenta below 2 GeV/c, rising to about 5% at 3.5 GeV/c.

III. ANALYSIS

The initial selection of semileptonic decay candidates follows the single-tag analysis described in Ref. [6]. For each $D^{*+} \rightarrow D^0 \pi^+$; $D^0 \rightarrow K^{(*)} e \nu$ candidate (charge conjugation is implied in all signal and tagging modes), we calculate the $D^{*+} - D^0$ mass difference $\Delta M = m(Ke\pi) - m(Ke)$ and the proper lifetime, as well as the output of an event selection neural network (NN). We then require that a high-momentum D decaying hadronically be fully reconstructed in the opposite hemisphere of the event. This ensures that the underlying production mechanism is $e^+ e^- \rightarrow c\bar{c}$ and provides a second production flavor tag. We implement additional candidate selection criteria based on studies of alternate background samples in data and a Monte Carlo (MC) simulated event sample (the ''tuning'' sample) to reduce various sources of background. The quark fragmentation in $e^+ e^- \rightarrow c\bar{c}$ MC events is simulated using JETSET [16], the detector response is simulated via GEANT4 [17], and the resulting events are reconstructed in the same way as are real data.

To minimize bias, we use a MC sample (the ''unbiased'' sample) disjoint from the tuning sample, to obtain all MC based estimates of efficiencies and backgrounds. We study this sample, with effective luminosity roughly equivalent to 603 fb^{-1} ($\approx 1.75 \times$ data) only after all selection criteria and the full analysis method have been established. After the expected background rates are determined from the unbiased MC, we examine the signal region in the data and determine the net number of observed RS and WS signal events (n_{RS} and n_{WS}). The measured mixing rate is then determined as $r_{mix} = n_{WS}/n_{RS}$, corrected for the relative efficiency of the WS and RS signal selection criteria.

A. Reconstruction and selection of semileptonic signal candidates

Semileptonic signal candidates are selected by reconstructing the decay chain $D^{*+} \rightarrow \pi^+ D^0$, $D^0 \rightarrow K^{(*)} e \nu$. There are no essential differences for this analysis between the K and $K^* \rightarrow K^\mp \pi^0$ modes, either theoretically or empirically, and thus no attempt is made to reconstruct the K^*—its charged K daughter is treated as if it were a direct daughter of the D^0. Approximately 11% of signal candidates accepted in the initial selection of semileptonic canidates [6] are in the K^* mode.

Identified K and e candidates of opposite charges are combined to create neutral candidate D decay vertices. Only candidates with vertex fit probability > 0.01 and invariant mass < 1.82 GeV/c^2 are retained. This requirement is imposed to exclude all hadronic two-body D^0 decays. The average PEP-II interaction point (IP), mea-

sured on a run-to-run basis using Bhabha and $\mu^+\mu^-$ events, is taken as the production point of D^0 candidates. The D^0 decay time is measured using the transverse displacement of the D^0 vertex from the IP and the D^0 transverse momentum due to the relative narrowness of the position distribution of the IP in the transverse $(r\text{-}\phi)$ plane [15]. Neural networks are used to estimate the boost of signal candidates in the $r\text{-}\phi$ plane, as discussed below.

The pions from D^{*+} decays are relatively soft tracks with $p_\pi^* < 450$ MeV/c, where the asterisk denotes a parameter measured in the e^+e^- CM frame. Charged tracks identified as either a charged K or e candidate are not considered as π candidates. To reject poorly reconstructed tracks, π candidates are required to have six or more SVT hits, with at least 2 hits in each of the $r\text{-}\phi$ and z views, and at least one hit on the inner three layers in each of the $r\text{-}\phi$ and z views. Pion candidates are refit constraining the tracks to originate from the IP, and are accepted only if the refit probability is greater than 0.01. Pion candidates meeting the above criteria are combined with Ke vertex candidates to form D^{*+} candidates.

A reasonable estimate of a signal candidate's proper decay time cannot be obtained using the partial reconstruction described above and, therefore, the three orthogonal components of the D^0 CM momentum vector are estimated with three separate JetNet 3.4 [18] neural networks. Each NN has two hidden layers, and is trained and validated with a large sample ($\mathcal{O}(10^5)$) of simulated signal events generated separately from the other MC samples used in the analysis. The following vector inputs to the NN's are used: $\mathbf{p}^* (Ke)$ (the momentum of the Ke pair constrained by the vertex fit), $\mathbf{p}^* (\pi)$, and the event thrust vector $\mathbf{T}^*$ (calculated using all charged and neutral candidates except the K and e candidates). For simulated signal events, the distribution of the difference between the true $\mathbf{p}^* (D^0)$ direction and the NN output direction is unbiased and Gaussian with $\sigma \approx 130$ mrad. The distribution of momentum magnitude differences shows an uncertainty of $\sigma_p/p \approx 10\%$ for a typical signal event.

The transverse momentum of a D^0 candidate and the projections of the IP and Ke vertex loci on the $r\text{-}\phi$ plane are used to calculate a candidate's proper decay time. The error on the decay time, calculated using only the errors on the IP and Ke vertex, is typically $0.8\tau_{D^0}$, where τ_{D^0} is the nominal mean D^0 lifetime. The contribution of the $\mathbf{p}^* (D^0)$ estimator to the total decay time uncertainty is approximately 10% and is ignored. Poorly reconstructed events, with calculated decay time errors greater than $2\tau_{D^0}$, are discarded, and only events with decay times between $-12\tau_{D^0}$ and $15\tau_{D^0}$ are retained. These criteria remove about 7% of the signal decays.

In addition to the above criteria, events are selected using a neural network trained to distinguish prompt charm signal from slow pion single-tag WS background events. The event selector NN uses a five-element input vector: p_{Ke}^*, p_π^*, $|\mathbf{T}^*|$, $\theta^*(\mathbf{p}_{Ke}^*, \mathbf{T}^*)$, and $\theta^*(\mathbf{p}_K^*, \mathbf{p}_e^*)$ where $\theta(\mathbf{a}, \mathbf{b})$ denotes the opening angle between the vectors $\mathbf{a}$ and $\mathbf{b}$. It has a single hidden layer of nine nodes and is also constructed using JetNet 3.4. Figure 1(a) shows the distribution of NN output for signal candidates, RS backgrounds, and WS backgrounds in double-tag unbiased MC events passing the semileptonic-side event selection criteria given above. The NN output is required to be greater than 0.9 in order to yield the best statistical sensitivity to WS signal events, assuming a null mixing rate, for the double-tag data set used here.

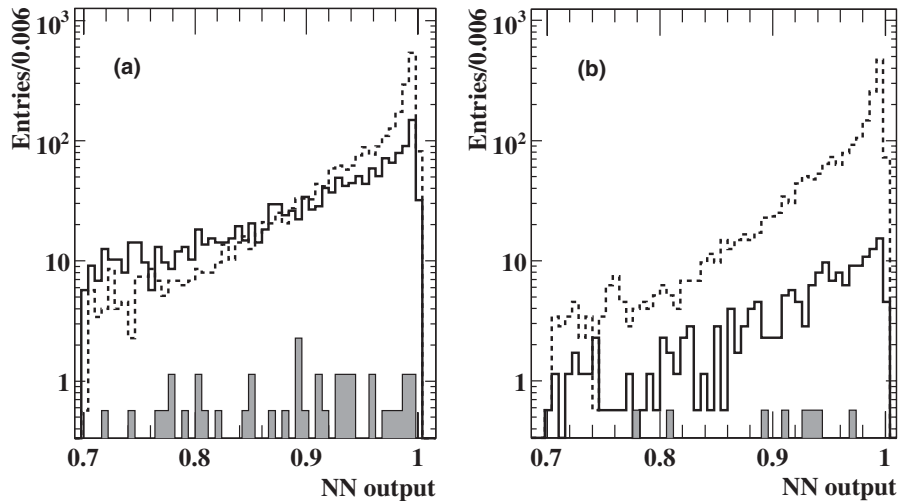FIG. 1. Event selector NN output, from double-tag luminosity-scaled unbiased MC, for events (a) passing the initial selection of semileptonic- side events and (b) passing the additional semileptonic-side selection criteria. The distributions shown are those for signal candidates (dashed line), RS backgrounds (solid line), and WS backgrounds (solid fill). The final event selection requires NN output >0.9.

B. The hadronic tagging samples

We use the flavor of fully reconstructed charm decays in the hemisphere opposite the semileptonic signal to additionally tag the production flavor of the semileptonic signal, and thus significantly reduce the rate of wrongly tagged candidates. We use five hadronic tagging samples. Three samples explicitly require D^{*+} decays: $D^{*+} \rightarrow D^0 \pi^+$ where $D^0 \rightarrow K^- \pi^+$, $D^0 \rightarrow K^- \pi^+ \pi^0$, and $D^0 \rightarrow K^- \pi^+ \pi^+ \pi^-$; while the other two samples are not related to D^{*+} decays: $D^0 \rightarrow K^- \pi^+$ and $D^+ \rightarrow K^- \pi^+ \pi^+$. The latter two decay modes are the only D^+ or prompt D^0 final states where tag yields are large enough and combinatoric backgrounds small enough to enable effective use for tagging. Candidates from the D^{*+} sample are explicitly excluded from the more inclusive $D^0 \rightarrow K^- \pi^+$ sample to ensure that the tagging samples are disjoint.

The selection criteria for the tagging samples, such as the ΔM ranges for the D^* modes or the use of production and decay vertex separation for the D^+ mode, vary from channel to channel to balance high purity against high statistics. Potential criteria are studied using candidate events from a RS sample chosen with loose requirements on the semileptonic side. To eliminate candidates from $B\bar{B}$ events, we require the CM momentum of the tag side D be at least 2.5 GeV/c. The individual D^{*+}, D^0, and D^+ tagging candidate invariant mass distributions for the final

RS sample are shown in Fig. 2. The purities of these tagging samples, defined as the ratio of signal in the selected mass range to the total number of candidates in that range (the darkly shaded entries in each histogram), vary from about 92% for $D^0 \rightarrow K^- \pi^+$ which do not come from D^{*+} to 97.5% for $D^0 \rightarrow K^- \pi^+$ from D^{*+}. In the very few events where there are multiple hadronic tag candidates, we use the tag coming from the highest purity tagging sample. We reject events with multiple semileptonic signal candidates, requiring that one and only one candidate, whether RS or WS, be present after all tagging and basic semileptonic-side selections are imposed. This requirement rejects approximately 13% of signal candidates and a similar fraction of background candidates.

C. Additional semileptonic-side selection criteria

Double-tagging the production flavor of the neutral D mesons effectively eliminates the WS background due to real semileptonic D decays paired with false slow pions from putative D^{*+} decay. From studies of background events in the tuning MC sample, we find that kaon and electron candidates are almost always real kaons and electrons, respectively, with correctly assigned charges. We also find that many fake slow pion candidates are electrons produced as part of conversion pairs, or Dalitz decays of π^0 or, to a much lesser extent, η mesons. These processes also
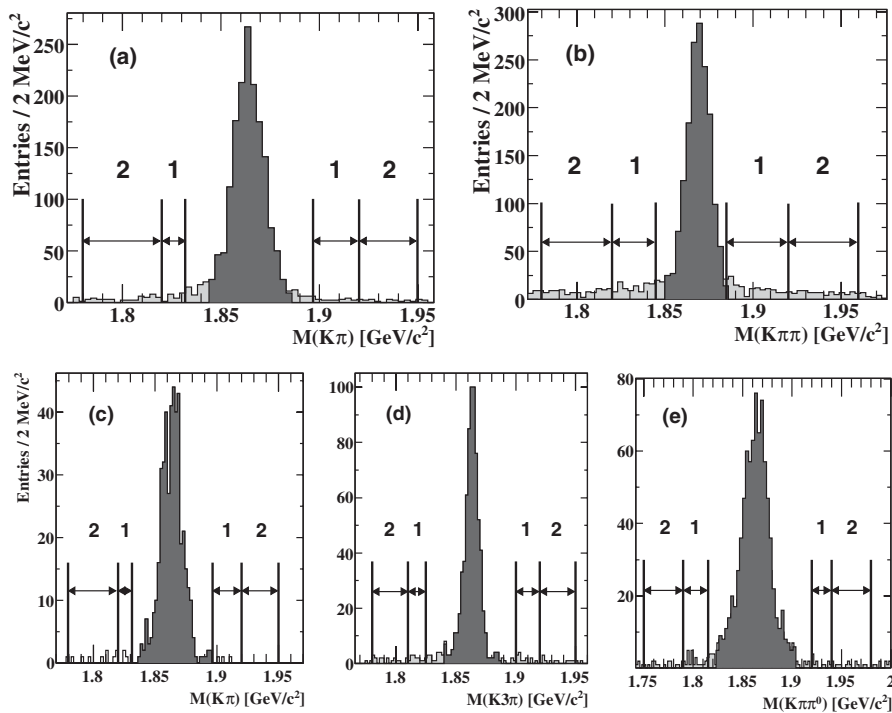
FIG. 2. Invariant mass distributions of hadronic tagging candidates in data events with RS semileptonic candidates passing the initial semileptonic-side selection. The dark shaded regions denote hadronic candidates used as tags. Sideband 1 events are used to characterize "false tag" rates and sideband 2 events are used for background normalization in optimizing the hadronic mass selection. Top row: (a) $D^0 \rightarrow K^- \pi^+$, (b) $D^+ \rightarrow K^- \pi^+ \pi^+$. Bottom row: $D^{*+} \rightarrow D^0 \pi^+$ events in final states (c) $D^0 \rightarrow K^- \pi^+$, (d) $D^0 \rightarrow K^- \pi^+ \pi^+ \pi^-$, (e) $D^0 \rightarrow K^- \pi^+ \pi^0$.

contribute background tracks to the pool of electron candidates used to create Ke vertices combinatorially. We consequently implement selection criteria to reject tracks which may have originated in such processes by requiring that neither an electron nor slow pion candidate form a conversion pair when combined with an oppositely charged track treated as an electron (whether identified as such or not). We further require that electron candidates not form a π^0 candidate when combined with a photon candidate and an oppositely charged track treated as an electron. (After applying all event selections, we find no contribution in the tuning MC sample from η Dalitz decays.) Rejecting photon conversions and Dalitz decays reduces the total RS and WS backgrounds by about 20% each, and has a negligible effect on signal efficiency.

To reduce backgrounds from kaons misidentified as electrons, we require that the laboratory momentum of electron candidates be greater than 600 MeV/c. This reduces the signal efficiency by about 15% and the background rate by about 35%. To further reduce the number of electrons that are considered as slow pions, we veto tracks where dE/dx in the SVT is consistent with that of an electron. This reduces the signal efficiency by about 15% and the background rate by about 25%.

We study kinematic distributions that discriminate between signal and background using data and MC events with two fully reconstructed hadronic decays of charm mesons. As a result, we require that the slow pion CM longitudinal momentum (along the axis defined by the direction opposite the tagging D's CM momentum) lie in the range 150–400 MeV/c and its transverse momentum be less than 80 MeV/c. This reduces the background by approximately 40% and the signal efficiency by approximately 15%.

We require that the electron-kaon invariant mass be greater than 800 MeV/c^2; this reduces the signal efficiency by a few percent while it reduces the background rate by approximately 20%. When we count the final number of signal candidates, we also require that $(M(Ke), \Delta M)$ lies inside the kinematic boundary expected for $D^{*+} \to D^0 \pi^+$; $D^0 \to Ke\nu$ decays where the neutrino
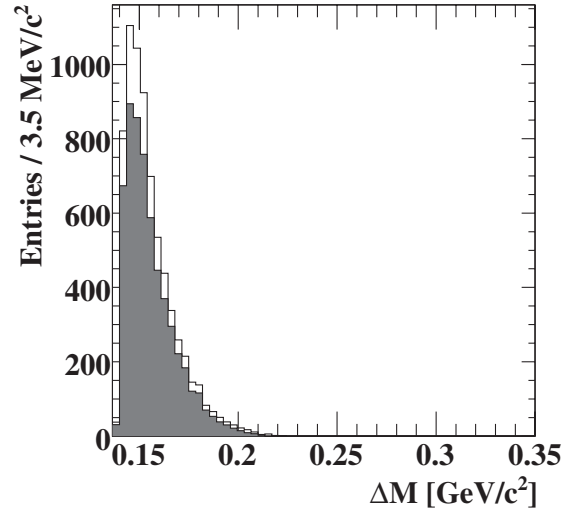

FIG. 3. RS signal ΔM distribution in unbiased MC scaled to the luminosity of the data before (line) and after (solid) applying the double-tag kinematic selection.

momentum is ignored. This has essentially no effect on signal efficiency, and reduces WS backgrounds by about 35%. The cumulative effects of the additional semileptonic-side selection criteria are summarized in Table II. (The selection for electron momentum $>$ 600 MeV/c is applied prior to calculating the acceptances listed in the table.) The effects of these additional selection criteria on $D^0 \to K^* e\nu$ events are reasonably consistent with those for $D^0 \to Ke\nu$ events. The combination of the slow pion longitudinal and transverse momenta and the $(M(Ke), \Delta M)$ selections will hereinafter be referred to as the "double-tag kinematic selection." Figure 3 shows the ΔM distributions of signal events in unbiased MC scaled to the luminosity of the data both before and after imposing the double-tag kinematic selection. The marginal efficiency resulting from applying these last selection criteria to signal events is 84 ± 1%.

The decay time distributions of the RS and WS signals should differ, as shown in Eq. (1). The RS sample is produced with an exponential decay rate, while the WS

TABLE II. Effects of additional semileptonic-side selection criteria. Approximate cumulative acceptance rates in the double-tag unbiased MC for signal and WS background as additional selection criteria are applied, relative to acceptances following the initial semileptonic-side selection. The signal acceptances are the same for RS and WS signal samples except for the decay time cut where the entry is that for the WS sample.

Criterion	Signal retained	WS background retained
$e^{\pm}$ conversion and Dalitz pair veto	100%	82%
π_s dE/dx cut	85%	66%
π_s p_T and p_L selection	72%	36%
$m(Ke) > 0.8$ GeV/c^2	71%	30%
$(M(Ke), \Delta M)$ kinematic cut	70%	20%
$600 < t < 3900$ fs	55%	10%

sample should be produced with the same exponential rate modulated by t^2. Figure 4 shows the normalized lifetime distributions for reconstructed simulated RS and WS signal events passing the final tag and signal-side selection. To improve sensitivity, we select only WS candidates with measured lifetimes between 600 fs($\approx 1.5\tau_{D^0}$) and 3900 fs($\approx 9.5\tau_{D^0}$), which accepts approximately 80% of signal and less than 30% of background. Because the RS signal-to-background ratio is comparatively very large, we accept RS candidates across the full range shown in Fig. 4. This WS/RS relative efficiency has a 2% systematic uncertainty due to imperfect knowledge of the decay time resolution function. This is determined from changes in the WS/RS efficiency observed when varying the signal resolution function according to the difference between resolution functions observed in RS data and MC samples.

Figure 1(b) shows the NN event selector output for RS signal, RS backgrounds, and WS backgrounds in the unbiased MC sample passing the additional semileptonic-side selection criteria (scaled to the luminosity of the data). The effectiveness of the additional semileptonic-side criteria in suppressing WS backgrounds while simultaneously retaining good signal efficiency can be seen by comparing Figs. 1(a) and 1(b). Figure 5 shows the ΔM distribution of WS backgrounds passing the decay time selection in unbiased MC scaled to the luminosity of the data both before and after the double-tag kinematic selection. A total of 2.85 background candidates, the sum of the luminosity-scaled events in the solid histogram shown in the figure, is expected after all event selection criteria are applied. The systematic uncertainty on this estimate is discussed below.
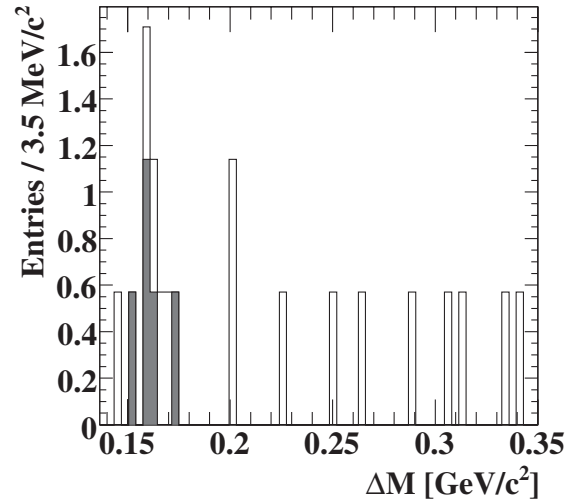
FIG. 5. WS ΔM distribution for background events passing the WS decay time selection in unbiased MC scaled to the luminosity of the data before (line) and after (solid) applying the double-tag kinematic selection.

D. Measuring signal yields

To determine the mixing rate, we first establish the number of RS signal candidates by fitting the RS ΔM distribution, as described in detail below. We then estimate the expected rate of WS background events in the signal region of the data from the unbiased MC sample. Using several background control samples drawn from both data and MC, we estimate how well MC events describe real data events. Using a statistical procedure with good frequentist coverage, we combine the number of candidates observed in the WS sample, the expected background rate, and the estimated systematic uncertainty in the expected background rate to obtain a central value for the mixing rate and 68% and 90% confidence intervals. This procedure is described in detail in the appendix.

We extract the number of RS signal events from the ΔM distribution of the RS sample selected without the double-tag kinematic selection using an extended maximum likelihood fit. The likelihood function includes probability density functions (PDF's) for the signal, the background events which peak in the signal region, and the combinatorial background. The PDF for each event class is assigned using the functional forms described in Ref. [6]. The shape parameters for the combinatoric background are determined using the following technique: D^0 signal candidates in the data from one event are combined with π_s candidates from another event to model the shape of this PDF. Based on MC studies, the shape of the peaking ΔM background is assumed to be the same shape as the signal. Its relative level is also determined from MC studies. The shape parameters of the signal PDF, as well as the number of RS signal events and the number of combinatorial background events, are then obtained from the likelihood
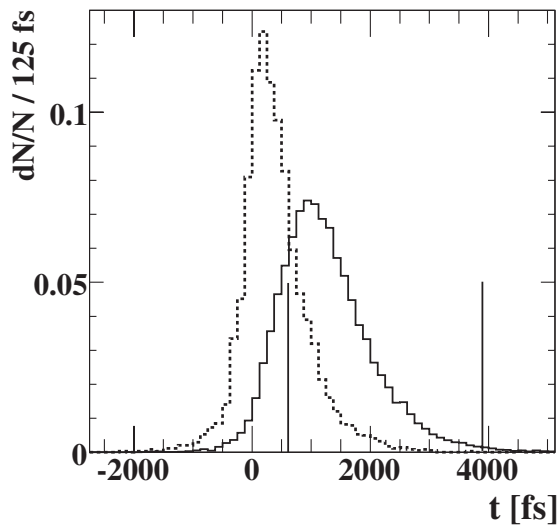

FIG. 4. Normalized RS (dashed line) and WS (solid line) reconstructed simulated signal lifetime distributions. The solid vertical lines mark the range for the selection of the WS events.

fit of the data. This procedure was validated using generic $e^+e^- \to c\bar{c}$ MC data sets.

The main plot in Fig. 6 shows the ΔM fit of the RS data before applying the double-tag kinematic selection, with the signal and background contributions overlaid. The fitted RS signal yield in this sample is 5748 ± 90 events, with $\chi^2 = 77$ for 60 bins, where six parameters are determined from the fit. The inset plot of Fig. 6 shows the RS data ΔM distribution after the double-tag kinematic selection is imposed. As noted above, the efficiency of this selection is 0.84 ± 0.01, giving a final RS signal yield of 4780 ± 94, which is used as the normalization in calculating the mixing rate.

To determine the number of WS mixed events, we consider three regions of ΔM: the signal region, $\Delta M \leq 0.20$ GeV/c^2; the near background region, $0.20 < \Delta M \leq 0.25$ GeV/c^2; and the far background region, $0.25 < \Delta M \leq 0.35$ GeV/c^2. These ΔM ranges are shown in Fig. 7, and are, respectively, labeled "1," "2," and "3" in the plot. To avoid potential bias, we examine neither the signal region nor the near background region in the WS data sample until all of the selection criteria and the procedure for calculating confidence intervals are determined. The WS signal region may contain both signal and background events after applying the final event selection criteria. As discussed above, we determine the expected number of background events from the unbiased MC sample: we observe 5 events, which scales to 2.85 for the luminosity of the data. To estimate the possible non-$c\bar{c}$ background rate, we also examine events which satisfy the semileptonic-side selection criteria but fail the tagging-side criteria because the mass of the hadronic D candidate falls outside the accepted window. Since we had examined the data events in the "far" sidebands (sidebands 2) of
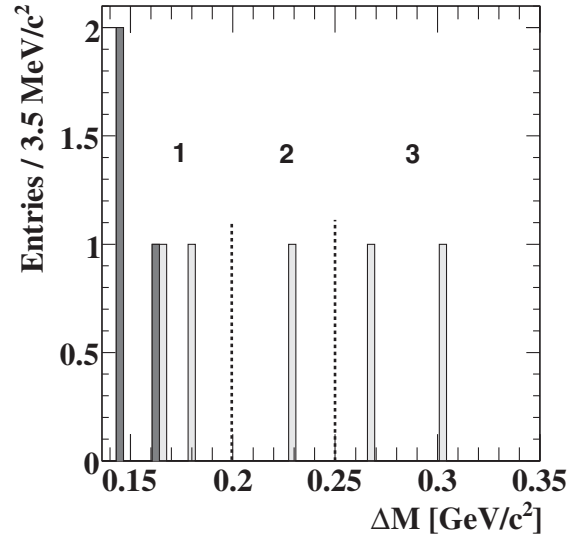
FIG. 7. WS data ΔM distribution. The dark histogram shows WS events in the data passing all event selection. The light histogram shows WS events passing all selections except the double-tag kinematic selection. Region 1 is the signal region, 2 is the near sideband, and 3 is the far sideband.

Fig. 2 while optimizing hadronic side selection criteria, we also examine those in the "near sidebands" (sidebands 1) to estimate the number of these "false tag" events: we find no WS candidates in the near or far ΔM sideband regions in either the data or unbiased MC sample. Given the agreement between data and the unbiased MC sample, we determine the central value of the number of WS signal events by subtracting the luminosity-scaled number of unbiased MC WS background events in the signal region from the number of candidates observed in the data there.

The dark shaded entries in Fig. 7 denote the ΔM distribution of WS candidates in the data after all event selection, where we observe 3 WS candidates in the signal region and none in the sideband regions. Given the expected WS background of 2.85 events shown in the solid histogram of Fig. 5, we calculate a net WS signal yield of 0.15 events. We discuss below the total error associated with the estimated number of WS background events.

E. Systematics and confidence intervals

To calculate confidence intervals for the number of mixed events observed, we first determine a systematic uncertainty associated with the WS background estimate. To do this, we compare 10 background control samples in data with the corresponding MC samples. The results of this comparison are shown in Table III. The first line compares the number of WS events observed in the far background region of the data and the tuning MC sample. The second line compares the same numbers for the data and for the unbiased MC sample. The remaining table entries compare the number of events observed in two types of doubly charged (DC) background samples ob-
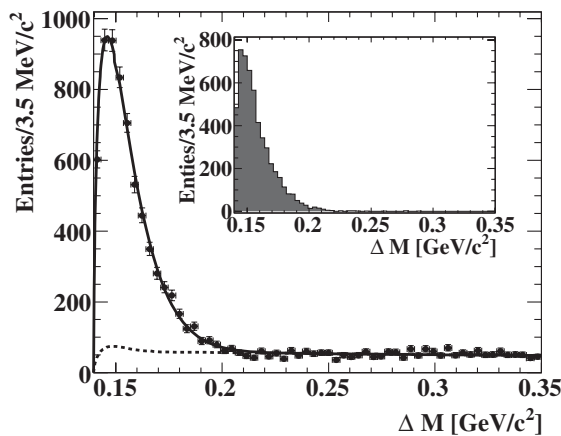

FIG. 6. RS data ΔM distribution. The main plot shows the RS data (points) before imposing the double-tag kinematic selection, and the projections of the total fit PDF (solid line) and the background PDF (dashed line). The inset plot shows the RS ΔM distribution after the double-tag kinematic selection criteria are applied.

TABLE III. Comparison of data and luminosity-scaled MC background yields. The doubly charged MC entries refer to MC event samples disjoint from those used to optimize event selection. The ''kinematic selection'' refers to the double-tag kinematic selection.

Entry	Data sample	ΔM Range (GeV/c^2)	Kinematic selection	Data	MC
1	WS, tuning MC	$0.25 \leq \Delta M \leq 0.35$	no	2 ± 1.4	2.1 ± 1.5
2	WS, unbiased MC	$0.25 \leq \Delta M \leq 0.35$	no	2 ± 1.4	3.4 ± 1.4
3	DC, OC	$\Delta M \leq 0.20$	yes	37 ± 6	40 ± 5
4	DC, SC	$\Delta M \leq 0.20$	yes	36 ± 6	51 ± 6
5	DC, OC	$\Delta M \leq 0.20$	no	42 ± 7	47 ± 6
6	DC, SC	$\Delta M \leq 0.20$	no	55 ± 8	64 ± 7
7	DC, OC	$0.20 < \Delta M \leq 0.25$	no	20 ± 5	24 ± 4
8	DC, SC	$0.20 < \Delta M \leq 0.25$	no	13 ± 4	19 ± 4
9	DC, OC	$0.25 \leq \Delta M \leq 0.35$	no	20 ± 5	31 ± 5
10	DC, SC	$0.25 \leq \Delta M \leq 0.35$	no	23 ± 5	18 ± 3

tained from data with those observed from the same sources in unbiased MC events. In both of the DC background samples, the kaon and the electron have the same charge sign, and are reconstructed exactly as neutral Ke vertex candidates are, except for the differing charge correlation. In those additionally labeled SC, the slow pion has the same charge as the kaon, while in those additionally labeled OC, the slow pion has the opposite charge.

Ignoring the correlations between entries 3,5 and 4,6 in Table III, we estimate the consistency between the data and MC samples by calculating a summed χ^2 for all the entries:

$$\chi^2(\text{data, MC}) = \sum_{i=1}^{10}\left[\frac{(x_i^{\text{data}} - x_i^{MC})^2}{(\sigma_i^{\text{data}})^2 + (\sigma_i^{MC})^2}\right] = 11.4. \quad (3)$$

The value $\chi^2 = 11.4$ is consistent with 1 per degree of freedom. Taken together, these observations indicate that the MC estimate for the background rate in the signal region of the WS sample is reasonably accurate. We conservatively assign the largest discrepancy between the data and MC rates, 50%, as the systematic uncertainty associated with the ratio between the MC estimate of the background rate and its true value.

To determine confidence intervals for the number of WS mixed events, we adapt a suggestion made in Ref. [19]. The complete statistical procedure is described in detail in the appendix; it is summarized here. We start with a likelihood function, $\mathcal{L}(n, n_b; s, b)$, for the number of events observed in the signal region of the WS data sample, n, and the corresponding number observed in the MC sample, n_b. $\mathcal{L}(n, n_b; s, b)$ depends upon the true signal rate s and the true background rate b in the signal region, and also accounts for the systematic uncertainty in the ratio of the true background rate in data to that estimated from MC. The value of (s, b) which maximizes the likelihood function, $\mathcal{L}_{\text{max}}$, is denoted by $(\hat{s}, \hat{b})$. As one expects naively, $\hat{b}$ is equal to n_b times the ratio of data and MC luminosities while $\hat{s} = n - \hat{b}$. We then search for the values of s where $-\ln\mathcal{L}(s)$ changes by 0.50 [1.35]; here $\mathcal{L}(s)$ denotes the likelihood at s maximized with respect to b. The lower and

upper values of s which satisfy this condition define the nominal 68% [90%] confidence interval for s. As discussed in the appendix, for the range of parameters relevant for this analysis, the confidence intervals produced by this procedure provide frequentist coverage which is accurate within a few percent.

F. Final results and conclusion

We observe 3 candidates for $D^0 - \bar{D}^0$ mixing compared to 2.85 expected background events. We ascribe a 50% systematic uncertainty to this expected background rate based on the largest statistically significant deviation (line 9) shown in Table III. We find the central value for the number of WS signal events to be 0.15, with 68% and 90% confidence intervals $(-2.2, 2.8)$ and $(-5.2, 4.7)$, respectively. Accounting for the ratio of WS and RS signal efficiencies due to the cut on the measured WS decay time (0.80 ± 0.02), we find the central value of r_{mix} to be 0.4×10^{-4}, with 68% and 90% confidence intervals $(-5.6, 7.4) \times 10^{-4}$ and $(-13, 12) \times 10^{-4}$, respectively. We ignore variations in the RS yield due to statistical error and systematic effects in the RS fit as they are negligible relative to the statistical errors associated with the WS data and MC rates as well as the 50% systematic error assigned to the ratio of MC and data WS background rates.

The sensitivity of this double-tag analysis is comparable to that expected for a single-tag analysis, see Table I. Future analyses should be able to combine these two approaches to significantly improve overall sensitivity to charm mixing using semileptonic final states. Improved methods for reconstructing and selecting semileptonic signal candidates, the use of more hadronic tagging modes, and the additional use of semimuonic decay modes may allow semileptonic charm mixing analyses to approach the r_{mix} sensitivity of analyses using hadronic final states.

ACKNOWLEDGMENTS

APPENDIX: STATISTICAL METHOD FOR ESTABLISHING CONFIDENCE INTERVALS

To estimate confidence intervals for the number of WS signal events, we adapt a method suggested in Ref. [19]. For a true signal rate, s, and background rate, b, in the WS signal region, we determine probability density functions (PDF's) for the number of background events we should observe in our Monte Carlo simulation, n_b, and the number of candidates we should observe in the WS signal region, n. We use these to define a global likelihood function for s and b which depends upon n and n_b: $\mathcal{L}(s, b; n, n_b)$. Given an observation (n, n_b), the central value for s is that which maximizes $\mathcal{L}(s, b; n, n_b)$. The boundaries of confidence intervals for s are then defined by the extremum signal rates in the (s, b) plane where the logarithm of the likelihood function changes by specified values based on those that would provide proper frequentist coverage in the limit of high statistics and Gaussian distributions. Assuming the PDF's we use are correct, we validate this algorithm by checking the frequentist coverage it produces for a range of values of s and b.

The PDF for n_b is taken to be

$$P(n_b; b_{\rm MC}) = N(b_{\rm MC}) \int_0^\infty \frac{x^{n_b}}{n_b!} e^{-x} \frac{1}{\sigma(b_{\rm MC})} \times e^{-(1/2)((b_{\rm MC}-x)^2/\sigma(b_{\rm MC})^2)} dx. \quad \text{(A1)}$$

In this equation, n_b and b are as defined above; $b_{\rm MC} = \alpha b$ is the mean number of events expected in a Monte Carlo simulation with α times the luminosity of the data sample, and $\sigma(b_{\rm MC}) = 0.5 b_{\rm MC}$ accounts for the

50% systematic uncertainty in the ratio of background rate in the data and background rate in the MC simulation. $N(b_{\rm MC})$ is the normalization such that $\sum_{n_b=0}^\infty P(n_b; b_{\rm MC}) = 1$.

The PDF for the combined observation (n, n_b) is then taken to be the product of $P(n_b; b_{\rm MC})$ and a purely Poisson term for n:

$$P(n; n_b) = P(n_b; b_{\rm MC} = \alpha b) \times \frac{(s + b)^n}{n!} e^{-(s+b)}. \quad \text{(A2)}$$

To obtain 90% (68%) confidence intervals, we use the following procedure.

(i) We write the global likelihood function for s and b as

$$\mathcal{L}(s, b; n, n_b) = P(n_b; b_{\rm MC} = \alpha b)$$
$$\times \frac{(s + b)^n}{n!} e^{-(s+b)}. \quad \text{(A3)}$$

(ii) We find the values $(\hat{s}, \hat{b})$ for parameters (s, b) which maximize the likelihood. These are $\hat{b} = n_b/a$ and $\hat{s} = n - \hat{b}$.

(iii) With $\mathcal{L}_{\max}$ the value of the likelihood at its maximum, we obtain 90% (68%) confidence intervals for s, by finding the points in the (s, b) plane where

$$\Delta \ln \mathcal{L} \equiv \ln \mathcal{L}_{\max} - \ln \mathcal{L}(s, b; n, n_b) = 1.35(0.50). \quad \text{(A4)}$$

(iv) We let s_l be the minimum value of s in this set and s_u be the maximum value. The 90% (68%) confidence intervals for s are the ranges (s_l, s_u).

We have determined the frequentist coverage of this algorithm for many values of (s, b) by using the PDF of Eq. (A3) to generate large samples of (n, n_b). For any one (s, b), we consider the ensemble of all (n, n_b) generated. For each of these (n, n_b) we determine whether s is contained in the 90% (68%) confidence interval defined using the algorithm described above. The fraction of all (n, n_b) containing the true value s is called the coverage. The coverage is therefore a function of both s and b as well as the level (68% or 90%). As a function of s between 0 and 10, and for fixed values of b between 2.5 and 7 (where 2.85 is the central value ''expected'' based on our observation of n_b), the coverages we calculate are close to the nominal values. In this range, the 68% intervals provide coverages between 64% and 72% with the most severe undercoverage observed for $s < 2$; the 90% intervals provide coverage between 87% and 92% with the most severe undercoverage again observed for $s < 2$. The deviations from nominal coverage are relatively small. We judge the statistical properties of the quoted intervals to be sufficiently accurate for this analysis.

[1] A. Datta and D. Kumbhakar, Z. Phys. C **27**, 515 (1985).

[2] A. A. Petrov, Phys. Rev. D **56**, 1685 (1997).

[3] G. Burdman and I. Shipsey, Annu. Rev. Nucl. Part. Sci. **53**, 431 (2003).

[4] A. A. Petrov (2003), arXiv:hep-ph/0311371.

[5] G. Blaylock, A. Seiden, and Y. Nir, Phys. Lett. B **355**, 555 (1995).

[6] B. Aubert *et al.* (*BABAR* Collaboration), Phys. Rev. D **70**, 091102 (2004).

[7] K. Abe *et al.* (Belle Collaboration), Phys. Rev. D **72**, 071101 (2005).

[8] C. Cawlfield *et al.* (CLEO Collaboration), Phys. Rev. D **71**, 077101 (2005).

[9] D. M. Asner *et al.* (CLEO Collaboration), Phys. Rev. D **72**, 012001 (2005).

[10] L. M. Zhang *et al.* (Belle Collaboration), Phys. Rev. Lett. **96**, 151801 (2006).

[11] B. Aubert *et al.* (*BABAR* Collaboration), Phys. Rev. Lett. **97**, 221803 (2006).

[12] B. Aubert *et al.* (*BABAR* Collaboration), Phys. Rev. Lett. **98**, 211802 (2007).

[13] M. Staric *et al.* (Belle Collaboration), Phys. Rev. Lett. **98**, 211803 (2007).

[14] B. Aubert *et al.* (*BABAR* Collaboration), Phys. Rev. Lett. **98**, 141801 (2007).

[15] B. Aubert *et al.* (*BABAR* Collaboration), Nucl. Instrum. Methods Phys. Res., Sect. A **479**, 1 (2002).

[16] T. Sjostrand *et al.*, Comput. Phys. Commun. **135**, 238 (2001).

[17] S. Agostinelli *et al.* (GEANT4 Collaboration), Nucl. Instrum. Methods Phys. Res., Sect. A **506**, 250 (2003).

[18] C. Peterson, T. Rognvaldsson, and L. Lonnblad, Comput. Phys. Commun. **81**, 185 (1994).

[19] F. C. Porter (*BABAR* Collaboration), arXiv:physics/0311092.